Received: 15 February 2019 | Revised: 12 April 2019 | Accepted: 15 April 2019

DOI: 10.1111/pce.13565

ORIGINAL ARTICLE

WILEY Plant, Cell & Environment

Direct comparison of four methods to construct xylem vulnerability curves: Differences among techniques are linked to vessel network characteristics

Martin D. Venturas[1] | R. Brandon Pratt[2] | Anna L. Jacobsen[2] | Viridiana Castro[2] | Jaycie C. Fickle[2] | Uwe G. Hacke[3]

[1] School of Biological Sciences, University of Utah, Salt Lake City 84112, Utah, USA

[2] Department of Biology, California State University Bakersfield, Bakersfield 93311, California, USA

[3] Department of Renewable Resources, University of Alberta, Edmonton, Alberta T6G 2E3, Canada

Correspondence
Martin D. Venturas, School of Biological Sciences, University of Utah, 257S 1400E, Salt Lake City, UT 84112, USA.
Email: martin.venturas@utah.edu

Funding information
Natural Sciences and Engineering Research Council of Canada, Grant/Award Number: Discovery Grant; Army Research Office of Department of Defense, Grant/Award Numbers: W911NF-16-1-0556 and 68885-EV-REP; National Science Foundation, Grant/Award Numbers: IOS-1252232, HRD-1547784 and IOS-1450650

Abstract

During periods of dehydration, water transport through xylem conduits can become blocked by embolism formation. Xylem embolism compromises water supply to leaves and may lead to losses in productivity or plant death. Vulnerability curves (VCs) characterize plant losses in conductivity as xylem pressures decrease. VCs are widely used to characterize and predict plant water use at different levels of water availability. Several methodologies for constructing VCs exist and sometimes produce different results for the same plant material. We directly compared four VC construction methods on stems of black cottonwood (*Populus trichocarpa*), a model tree species: dehydration, centrifuge, X-ray–computed microtomography (microCT), and optical. MicroCT VC was the most resistant, dehydration and centrifuge VCs were intermediate, and optical VC was the most vulnerable. Differences among VCs were not associated with how cavitation was induced but were related to how losses in conductivity were evaluated: measured hydraulically (dehydration and centrifuge) versus evaluated from visual information (microCT and optical). Understanding how and why methods differ in estimating vulnerability to xylem embolism is important for advancing knowledge in plant ecophysiology, interpreting literature data, and using accurate VCs in water flux models for predicting plant responses to drought.

KEYWORDS

centrifugation, dehydration, droughts, plant stems, poplar, *Populus*, trees, X-ray microtomography

1 | INTRODUCTION

To avoid dehydration, trees need to replenish the water they lose through their leaves when they open their stomata to acquire CO_2 for photosynthesis. They achieve this by transporting water from the soil to the leaves through specialized conduits in the xylem under negative pressures (Dixon & Joly, 1895). This transport system is energetically efficient but can be compromised if an air bubble is sucked into a conduit, expands, and spreads through the conduit network generating emboli that block water transport, in a process called cavitation (Sperry & Tyree, 1988; Zimmermann, 1983). Cavitation is more prominent during periods of drought and can lead to reductions in productivity and plant mortality, and it may slow postdrought recovery (Adams et al., 2017; Brodribb & Cochard, 2009; Sperry, Hacke, Oren, & Comstock, 2002; Tyree & Sperry, 1988). Thus, xylem vulnerability to cavitation is a critical trait for understanding and predicting forest responses to drought and to global climate change (Mencuccini, Manzoni, & Christoffersen, 2019; Sperry & Love, 2015; Sperry et al., 2017; Venturas et al., 2018).

Vulnerability curves (VCs) usually represent the loss of hydraulic conductivity of an organ due to emboli as xylem pressure declines. There are several methods for evaluating xylem resistance to cavitation, which differ in the techniques used for (a) submitting samples to water stress and (b) evaluating the loss in conductivity (reviewed in Cochard et al., 2013; Venturas, Sperry, & Hacke, 2017). For some species, studies have reported very different curves depending on the technique used for constructing VCs. In some cases, differences can be due to heterogeneity among plant materials used for evaluating xylem resistance to cavitation, time of year, developmental stages, interpopulation variability, or sample preparation (see discussion in Hacke et al., 2015). In others, it can be due to measurement artefacts as shown for the flow-centrifuge method, also known as "Cavitron" (Cochard et al., 2005; Wang, Zhang, Zhang, Cai, & Tyree, 2014). However, in some cases, differences may reflect that different techniques measure different xylem properties; thus, the measured parameters from different VC methods may not be directly comparable. Measurement of different xylem properties, which depend on species-specific xylem conduits network characteristics, may lead to differences in the appearance of VCs from different methods. The motivation of this study was to examine the potential cause of method discrepancies, because understanding these potential differences between techniques is essential for accurately interpreting VCs and applying the information obtained from VCs to plant physiology (Venturas et al., 2017).

In this study, we compared two commonly used techniques for inducing xylem embolism, air dehydration (Sperry, 1986; Tyree, Alexander, & Machado, 1992), and the standard centrifuge method (Alder, Pockman, Sperry, & Nuismer, 1997; Pockman, Sperry, & O'Leary, 1995). Air dehydration, also termed benchtop dehydration, involves drying down whole plants or excised organs so that xylem pressure decreases over the course of hours to days. The standard centrifuge method rapidly produces a pressure drop in the centre of excised xylem samples that can be calculated as $P_{min} = -0.5\rho\omega^2r^2$, where ρ is the density of water, ω is the angular velocity, and r is the distance from the axis of rotation to the meniscus of the rotor reservoir (Alder et al., 1997). These embolism induction techniques were combined with three different techniques for evaluating losses in conductivity: (a) the hydraulic conductivity apparatus (Sperry, Donnelly, & Tyree, 1988), (b) X-ray–computed microtomography (microCT; Brodersen, McElrone, Choat, Matthews, & Shackel, 2010; Fromm et al., 2001), and (c) the optical visual technique (Brodribb, Carriqui, Delzon, & Lucani, 2017). Hydraulic conductivity measures directly quantify flow through the xylem, whereas both microCT and the optical technique rely on assessment of visual data. Prior studies have compared some of these techniques, but results of these comparisons have been variable. Some studies have found similar VCs constructed using microCT and hydraulic conductivity measures (e.g., Losso et al., 2019; Nardini et al., 2017; Nolf et al., 2017), whereas others found significant differences (e.g., Cochard, Delzon, & Badel, 2015; López et al., 2018). The optical visual technique is relatively new; thus, it has been less tested against other methods, and some studies suggest that it provides very different VCs compared with other techniques, particularly when applied to angiosperms with variable vessel diameters (Brodribb et al., 2017; Skelton et al., 2018).

Conduit network characteristics may explain differences among VCs constructed with different methods. One of the main differences is in whether conductivity is measured directly (hydraulic methods) and estimated based on theoretical calculations (microCT) or based on a proportion of observed events (optical). Within the xylem tissue, the impact of an embolus on conductivity through the network is difficult to calculate due to flow-path resistance changes linked to intricacies in conduit connectivity and pit membrane resistances (Jacobsen & Pratt, 2018; Mrad, Domec, Huang, Lens, & Katul, 2018), leading to potential discrepancies between theoretical conductivity and actual conductivity. Conduits of different diameters also contribute differentially to flow, so the use of events to estimate hydraulic function is problematic, especially if events are each considered to be equal in their influence on conductivity (Brodribb et al., 2017). Some of these potential differences may be minimized in xylem tissue composed of relatively homogenous conduits. Therefore, we decided to examine the differences between methods for constructing VCs for a short-vesselled, diffuse-porous species, which should be less prone to measurement discrepancies.

The main objectives of this study were to (a) directly compare VCs constructed with different methods on the same plant material, (b) test for potential artefacts in the different methods, and (c) determine if the patterns observed fall within theoretical expectations. We also analysed if primary xylem vessels were more vulnerable to cavitation than secondary xylem vessels, because this could be important for 1-year-old stems and in the comparison of data from young stems to older tissue. We constructed VCs with four different techniques (dehydration, centrifuge, microCT, and optical) on stems of black cottonwood (*Populus trichocarpa* Hook.), a short-vesselled, diffuse-porous species. Direct comparisons were performed whenever possible; that is, measurements were performed on the exact same samples.

2 | MATERIAL AND METHODS

2.1 | Plant material

We performed this study with black cottonwood because this species has short vessels (mean vessel length is approximately 2 cm; Jacobsen et al., 2018; Venturas et al., 2016). In addition, this is a model species that has previously been used to compare VC techniques (e.g., Jacobsen et al., 2018; Venturas et al., 2016) or VCs among populations (e.g., Sparks & Black, 1999). Cottonwood trees were grown at the Environmental Studies Area at California State University, Bakersfield, USA (35.3474°N, 119.0994°W, 113 m above sea level). Saplings (originally planted from seed) were planted in spring 2014 in the nodes of a 4 × 4-m square grid (full details of plot design in Jacobsen et al., 2018). Cottonwood trees were 11 years old and over 6-m tall when they were sampled late June to early July 2018. The plot was well irrigated during the whole growing season.

2.2 | Xylem pressures of intact plants in the field

Sampled trees had not suffered water stress during the growing season, and their predawn water potential, measured with a pressure chamber (Model 2000, PMS Instrument Company, Albany, OR, USA), was approximately −0.2 MPa. Stem xylem native embolism of the current year growth is determined by the minimum pressure that samples experience at midday when leaves are transpiring. Thus, we measured midday xylem pressures of transpiring and nontranspiring leaves (on June 29) on a hot and sunny day to determine the minimum pressure that the stem xylem from the current year growth was experiencing during the experimental period in intact plants and the pressure drop in leaves. We covered three leaves per tree (six trees in total) at predawn with resealable plastic bags covered with tin foil to prevent transpiration. At midday, we measured the xylem pressure of the covered leaves (in equilibrium with stem xylem) and of adjacent transpiring leaves within each branch.

2.3 | VC methods comparison

We designed the experiment so that identical or equivalent plant material was used for methods comparisons (Table 1). The four methods we tested varied in the techniques used for inducing cavitation (air dehydration vs. centrifugation) and/or measuring cavitation (conductivity apparatus vs. micro-CT vs. optical). Throughout this paper, we will refer to the four VC construction methods as Dehy-CondApp (air dehydration + conductivity apparatus), Dehy-MicroCT (air dehydration + micro-CT), Cent-CondApp (centrifugation + conductivity apparatus), and Dehy-Optical (air dehydration + optical visual technique).

2.3.1 | Dehy-CondApp and Dehy-MicroCT curves

We collected large branches (>2-m long) at predawn (cut in air) from the outer canopy of six randomly selected trees within the plot. We immediately inserted the branches in two opaque bags with a piece of moist paper cloth and transported them to the laboratory 0.5 km away (<30 min). In the laboratory, we selected a distal shoot of current year's growth (~50-cm long and containing a terminal bud) and individually covered with small resealable bags four to five leaves not contained within the selected shoot. We let the branches air-dry for different time periods (0–48 hr) in order to reach a wide range of water potentials for constructing VCs. After air dehydration, we double bagged the large branches for over 2 hr to allow xylem pressure to equilibrate within the sample. We used a pressure chamber to estimate stem xylem pressure as the mean pressure of the covered leaves. We excised the selected shoot under water at ~60 cm from the terminal bud and trimmed it back to 50 cm by performing several cuts with a sharp razor to avoid inducing cavitation during sample preparation (Venturas, MacKinnon, Jacobsen, & Pratt, 2015). We placed the cut end in a test tube with water.

Samples were then prepared for microCT scanning. We used a gold pen to mark the section where the stem would be scanned (the paint is easily detected in microCT images). The mean stem diameter was 4.06 mm (±0.55 *SD*; n = 15). We wrapped the shoot with plastic film to halt transpiration during measurements and to stabilize it while measuring native-state embolism in the microCT. Shoots were mounted vertically in the microCT system stage (Model 2211, Bruker Corporation, SkyScan, Billerica, MA, USA). Scans were performed at 40 kV and 600-μA energy at a resolution of 3 μm. Two scans were made along the length of each stem, and they were stitched together using software during the reconstruction step (InstaRecon, Champaign, IL, USA). This protocol resulted in images for the whole cross section and a length of 6.5–9.0 mm. It took 18–30 min to fully scan each sample. Some measures from these scans, including the vessel length distribution from the scanned segments, vessel diameter measures, and percent loss in conductivity (PLC) estimates from conductivity and microCT, have been previously reported in Jacobsen, Pratt, Venturas, and Hacke (2019).

Immediately after the microCT scan was performed, we excised, under water, a 14-cm segment containing the scanned region in its centre. We trimmed the ends under water with a razor blade and connected the sample to a conductivity apparatus (Sperry et al., 1988). The sample had hydrated xylem pressures (close to 0) at this point because the cut end had been under water during scanning and the leaves were covered in plastic to minimize transpiration. This should have minimized, if not eliminated, any cutting artefacts (Venturas et al., 2015). We performed measurements with a degassed ultrafiltered 20mM KCl solution (in-line filter Calyx Capsule Nylon 0.1 μm, GE Water and Process Technologies, Trevose, PA, USA) and a low-pressure difference (2–3 kPa). Initial conductivity (K_h) was calculated as the flow rate divided by the pressure and multiplied by the segment length. Measurements were corrected for background flow due to passive water uptake when the pressure driving flow is 0 kPa (Hacke, Sperry, & Pittermann, 2000). We flushed samples for 1 hr with degassed 20 mM KCl solution at 100 kPa to reverse all embolism and measured maximum hydraulic conductivity (K_{hmax}). In all cases, flushing led to an increase in K_h suggesting that stems were not irreversibly occluded with substances like gels or debris and further suggesting that emboli were the chief cause for K_h declines. We calculated the specific conductivity (K_s) and maximum specific conductivity (K_{smax}) by dividing K_h and K_{hmax}, respectively, by the cross-section area of the distal end of the segment (including bark). We calculated the percent loss in hydraulic conductivity of each sample as follows:

$$PLC = 100^{*}\left(1 - \frac{K_h}{K_{hmax}}\right). \quad (1)$$

After K_{hmax} was measured, we excised a 1-cm segment containing the scanned section, which had been marked prior to scanning. We connected tubing to the basal end of the 1-cm–long segment and blew dry nitrogen gas through the sample for 5 min at 100 kPa. This method pushes water out of open vessels and also dehydrates the short sample so that all vessels of the segment become embolized (Jacobsen et al., 2019; McElrone, Choat, Parkinson, MacDowell, & Brodersen, 2013). We scanned the 1-cm segment in the microCT with the same settings

TABLE 1 Experimental design followed for comparing vulnerability curve construction techniques

Technique	Steps
Dehy-CondApp and Dehy-MicroCT	1. Collected branches (>2 m) at predawn (n = 15) 2. Air-dried them in the laboratory for 0–48 hr 3. Bagged four leaves and double bagged the branch for >2 hr 4. Measured xylem pressure of four leaves in a pressure chamber 5. Excised the terminal shoot (50 cm) under water, placed it in a test tube with water, marked area to be scanned, and wrapped it in plastic film 6. Scanned the stem in the microCT (microCT Scan 1) 7. Excised 14-cm segment under water with scanned region in the centre 8. Measured native conductivity (K_s) with conductivity apparatus 9. Flushed sample for 1 hr to reverse embolism 10. Measured maximum conductivity (K_{smax}) with conductivity apparatus 11. Excised 1-cm segment containing scanned region and blew dry gas into it for 5 min at 100 kPa 12. Scanned the 1-cm gas–dried segment in microCT (microCT Scan 2) 13. Processed scanned images 14. Measured all gas-filled vessels from Scans 1 and 2 to establish microCT K_{ts} and K_{tsmax} 15. Calculated percent loss in conductivity (PLC) for both techniques 16. Constructed K_s or K_{ts} and PLC vulnerability curves
Cent-CondApp	1. Collected branches (>1 m) at predawn; cutting under water (n = 12) 2. Excised 14-cm segments under water 3. Flushed segments for 1 hr to reverse embolism 4. Measured K_{smax} with the conductivity apparatus 5. Spun stem segments for 6 min at −0.5 MPa in the standard centrifuge 6. Measured K_s after the spin with the conductivity apparatus 7. Calculated PLC for that pressure 8. Repeated steps 5 and 6 for decreasing xylem pressures (−1.0, −1.5, −2.0, −3.0, and −4.0 MPa) 9. Constructed the K_s and PLC vulnerability curves
Dehy-Optical	1. Collected branches (>2 m) at predawn (n = 6) 2. Covered some leaves of the branch with individual resealable bags 3. Measured the xylem pressure of two leaves 4. Peeled the bark to expose xylem of the terminal shoot and covered it with silicone vacuum grease 5. Secured the sample against the wall 6. Took one photograph of the debarked section every 2 min 7. Sampled bagged leaves at different time intervals to evaluate the xylem pressure of the branch 8. When leaves wilted, we stopped taking photographs 9. Imaged in the microCT the debarked section 10. Fitted a curve to represent xylem pressure versus time and assigned a pressure to each photograph 11. Created a video with all the images of each stem 12. Visualized the videos and counted the light change events that occurred for each video frame 13. Constructed the cumulative distribution of events relative to xylem pressure, similar to PLC curve
Single-spin centrifuge and microCT	1. Collected branches (>1 m) cutting under water at predawn (n = 6) 2. Excised 14-cm segments under water 3. Measured initial K_s with a conductivity apparatus 4. Spun the samples for 6 min at −3.0 MPa 5. Measured K_s with a conductivity apparatus 6. Cut the 14-cm segment under water into three 4.5-cm segment (proximal, central, and distal) 7. Measured K_s of each segment with a conductivity apparatus 8. Scanned the centre of the central segment in the microCT for establishing K_{ts} at −3 MPa 9. Flushed the segments with degassed solution for 1 hr 10. Measured K_{smax} of each segment with a conductivity apparatus 11. Excised the 1 cm containing the scanned region and blew dry gas into it for 5 min at 100 kPa 12. Scanned the gas-dried segment in the microCT for establishing K_{tsmax} 13. Compared K_s and K_{ts} of the 14-cm segments from centrifuge and microCT and compared their PLC 14. Compared conductivity apparatus K_s and PLC of proximal, central, and distal 4.5-cm segments

Abbreviations: Dehy-CondApp, air dehydration plus conductivity apparatus; Dehy-MicroCT, air dehydration plus x-ray computed microtomography; Cent-CondApp, standard centrifuge method plus conductivity apparatus; Dehy-Optical, air dehydration plus optical visual technique; K_s, specific conductivity; K_{smax}, maximum specific conductivity; K_{ts}, theoretical specific conductivity; K_{tsmax}, maximum theoretical specific conductivity; PLC, percent loss in conductivity.

as described above. This second scan of each segment was performed for visualizing all the vessels contained within a segment, as gas-filled vessels are easy to distinguish from cell walls in microCT images.

For constructing the microCT VC, we calculated the theoretical hydraulic conductivity (K_t) with the Hagen–Poiseuille equation, assuming xylem conduits to be circular (Lewis & Boose, 1995):

$$K_t = \frac{\varphi \cdot \pi}{128 \cdot \mu} \cdot \sum_{i=1}^{n} D_i^4, \quad (2)$$

where φ is water density (kg m^{-3}), μ water dynamic viscosity (MPa s), and D_i the diameter of the n vessels of the cross section (m). The diameter of each vessel was calculated as the diameter of a circle with an area equivalent to the area of the vessels' lumen. We selected one cross section from the same point where we sampled the stem in its native state, and we obtained the diameters of all air-filled vessels contained within the cross section with an automated analysis performed with CTAn software (Bruker Corporation, Billerica, MA, USA). We estimated maximum theoretical hydraulic conductivity (K_{tmax}) by applying Equation (2) to the measured diameters from the microCT images of gas-dried segments (second scan). We calculated K_t of embolized vessels (K_{temb}) from the corresponding cross section from the native scan (first scan) and estimated theoretical initial conductivity (K_t) as K_{tmax} minus K_{temb}. We obtained microCT theoretical specific conductivity (K_{ts} and K_{tsmax}) by dividing K_t and K_{tmax} by the cross-sectional area of the section imaged (with bark). We used Equation (1) to calculate microCT percent loss in theoretical conductivity. We standardized both conductivity apparatus measurements and theoretical conductivity calculations to 22°C (φ = 997.8 kg m^{-3}; μ = 9.544 × 10^{-10} MPa s). Sample size for constructing the Dehy-CondApp and Dehy-MicroCT curves was n = 15 (15 branches from six trees).

Estimating K_t, this way assumes that all vessels that can be gas dried are functional in the initial state. We tested this assumption by feeding an iodine-rich compound (iohexol) or crystal violet to the transpiration stream of some branches for 2 hr. These chemicals are taken up and move through the functional conduits in the vascular system (Pratt & Jacobsen, 2018). These tests, as well as examination of sample cross sections using fluorescence imaging, showed that this assumption was valid for this species at the time we sampled our plants (see Jacobsen et al., 2019).

Prior studies have indicated that X-ray scanning of samples may lead to damage (Petruzzellis et al., 2018; Savi et al., 2017). To test for potential impacts of scanning on our hydraulic conductivity measures, we conducted a test where we measured K_h, then scanned samples as described above, and then remeasured K_h (n = 3 stems). A difference in K_h before and after scanning would indicate that damage to the xylem tissue may have impacted our measures, whereas no difference would indicate that our scanning time and settings were not leading to artefacts in our hydraulic conductivity measurements.

In addition to the measures above for Dehy-MicroCT samples, we conducted an analysis of microCT images that separately analysed the degree of embolism in the primary and secondary xylem tissues of the scanned stems. This was done to evaluate if there was a difference in the cavitation resistance of primary xylem vessels compared with secondary xylem. We identified primary xylem vessels (which are located in the regions adjacent to the vertices of the pith pentagon) and measured their K_t and K_{tmax}. We calculated secondary xylem K_t as the whole section K_t minus primary xylem K_t. We calculated secondary xylem K_{tmax} the same way. We constructed and compared the VCs for primary and secondary xylem.

2.3.2 | Cent-CondApp curve

We constructed the centrifuge VC with samples from the same trees and equivalent in size and location within the branch to those used for the Dehy-CondApp and Dehy-MicroCT curves. We excised branches (>1-m long) under water at predawn and transported them to the laboratory with their cut end submerged in water. We excised a 14-cm segment from each branch under water and shaved its ends with a razor blade. The mean diameter at the centre of these segments was 4.22 mm (±0.71 *SD*; n = 12). We flushed the segments for 1 hr at 100 kPa with a 20mM KCl-degassed solution and used the conductivity apparatus to measure their K_{hmax}. We used the rotor and reservoir design of the standard centrifuge method (Alder et al., 1997). We introduced foam pads in the degassed solution reservoirs to avoid the segment ends being exposed to air when the rotor was not spinning (Tobin, Pratt, Jacobsen, & De Guzman, 2013). Stems were progressively spun for 6 min at increasing rotational velocities that corresponded to pressure drops in the centre of the segment of −0.5, −1.0, −1.5, −2.0, −3.0, and −4.0 MPa. After each pressure drop, we measured K_h and calculated PLC (Equation 1).

An additional set of six segments (14-cm long) was used to evaluate the centrifuge method and directly compare this method to microCT. We collected and prepared samples following the same procedure as for the centrifuge curve. We measured native K_h, and as trees were highly hydrated due to consistent irrigation, we considered that value to represent K_{hmax} (i.e., we did not flush this set of six samples for measuring K_{hmax}). We spun the segments for 6 min at −3.0 MPa using the standard centrifuge (Alder, Sperry, & Pockman, 1996; Tobin et al., 2013). We selected −3.0 MPa because the previous curve showed PLC ≈ 100 at this pressure. We measured K_h of the whole segment and calculated PLC (Equation 1). We covered both ends of the segments with test tubes containing water and placed them vertically in the microCT stage. We scanned the segments at their centre (where maximum pressure drop is reached in the centrifuge) for calculating their K_t at −3.0 MPa. Next, we cut with a razor blade each 14-cm segment under water into three 4.5-cm–long segments (proximal, central, and distal). We measured K_h of each one of these segments with the conductivity apparatus. The segments were then flushed for 1 hr at 100 kPa with a 20mM KCl-degassed solution, and the K_{hmax} of each segment was measured. We calculated PLC for each segment. We performed this experiment to test if the profile of loss in hydraulic conductivity matched theoretical expectations, that is, if the centre segment, where there is a larger pressure drop during centrifugation, showed higher PLC than the proximal and distal segments (Hacke et al., 2015; Sperry, Christman, & Smith, 2012; Tobin et al., 2013), which sometimes has not been found with the Cavitron method (Cochard et al., 2005). Finally, we excised the central 1-cm segment from the centre 4.5-cm segments. We gas dried the segments as previously described, and we rescanned them for calculating K_{tmax}. We used the same microCT settings and followed the same procedures for analysing the images as described for the Dehy-MicroCT VC.

2.3.3 | Dehy-Optical curve

An optical method was used to independently assess vulnerability to cavitation (Brodribb et al., 2017). We collected large branches (>2 m) from the same trees at predawn following the same protocol as for the dehydration curve and transported them to the laboratory with their cut ends in water (<10 min). We selected a terminal current year shoot equivalent to the ones used for the other methods. We covered all the leaves and shoots individually with resealable bags and allowed the large shoot to fully hydrate for at least an hour. During this time, we carefully removed a portion of bark (about 5 × 5 mm) while keeping the area moist by dripping water onto the region. Removal of the bark was done to expose a region of xylem to photograph during drying. We tested covering the exposed xylem with water soluble ultrasound gel (Medvat Clear Transmission Gel, MYT Enterprises, Lakewood, NJ, USA), but that did not prevent the exposed area from drying rapidly and deforming in the debarked region. Thus, we used clear silicone vacuum grease (4, Dow Corning Company, Midland, MI, USA) for covering the exposed xylem immediately after removing the bark for avoiding its desiccation and deformation. We secured the branch against a wall with adhesive tape. We took a picture at 2-min intervals of the stem section from which the bark was removed (Fujifilm XT-2 camera, Fujifilm Corporation, Tokyo, Japan) with a macro lens attached (Mitakon Creator 20-mm f/2, Zhong Yi Optics, Shenyang City, China). We measured the xylem pressure of three to four bagged leaves with a pressure chamber at the beginning of the curve (first photograph) and at different time intervals (15 min to 12 hr) during the dry-down until leaves wilted. Our benchtop dry-down was performed in a closed room under low light conditions (dark or <15 PAR). Therefore, it was progressive and slow (31 to 50 hr), and covered leaves were in equilibrium with the stem xylem pressure. We fitted the water potential versus time of each branch to a six-power polynomial curve for estimating the water potential of the branch for each photograph. For each branch, we constructed a time-lapse video that was one frame per second (Photoshop CC, Adobe, San Jose, CA, USA). BatchPhoto software (BatchPhoto, Bit&Coffee Ltd., Craiova, Romania) was used to place a date and time stamp on each image. Videos were viewed, and "optical events" were recorded along with the date and time. Each event represented a change in the colour of pixels of a region within the recorded images (Brodribb et al., 2017). There were also largely observable embolism events where we could see gas bubbles forming in cells. We evaluated our visual scoring technique by having multiple viewers evaluate and score the same video sequences. There was strong agreement in the shape of these response curves between three independent observers (Figure S1); however, there was not perfect agreement on the total number of events tabulated by each observer. We represented the optical VC as the percent of cumulative total events as the water potential becomes more negative.

After the optical curve was performed, we microCT scanned the samples just above the debarked section (in one stem) and in the debarked area that was observed during the optical measurements (settings as described above) for all of the six stems. This enabled us to observe the sampled tissue to assess its status.

2.4 | Statistical analyses

We fitted data from the Dehy-CondApp, Dehy-MicroCT, and Cent-CondApp VCs to Weibull functions that represent K_s and PLC as a function of xylem pressure (P):

$$K_s(P) = K_{smax} \cdot e^{-\left(\frac{-P}{b}\right)^c}, \quad (3)$$

$$PLC(P) = 100 \cdot \left(1 - e^{-\left(\frac{-P}{b}\right)^c}\right), \quad (4)$$

where b and c are, respectively, the Weibull scale and shape parameters. We used bootstrapping for propagating the uncertainty of the datasets and calculating the 95% confidence intervals (CIs) of VCs. This was performed by resampling with replacement the dataset to obtaining 1,000 samples of equal size and fitting each sample to the curve by least square mean errors. The percentiles 2.5 and 97.5 for each pressure of all fits were established as the 95% CIs. For the optical method, we used Equation (4) for fitting the cumulative percent of events. We resampled whole curves (each sample) for centrifuge and optical methods as points within them are not independent. The pressure at which 50% loss in conductivity is reached (P_{50}) was obtained from the fitted curves. Curve fitting and CI calculation were performed in R (R Core Team, 2016).

Additional t test and paired t test (for paired samples) comparisons among K_s and PLC of different methods were performed with Sigma Plot 13.0 (Systat Software Inc., San Jose, CA, USA). If t-test equal variance requirement was not achieved, the comparison was performed with a Mann–Whitney rank sum test (MWRST). We used an analysis of variance (ANOVA) when three or more groups were compared (e.g., proximal, central, and distal segments). We performed a Kruskal–Wallis one-way analysis of variance on ranks test when ANOVA's equal variance among groups requirement was not met. Tukey's Honest Significant Difference test was used to compare groups when variance analyses indicated significant differences among them.

3 | RESULTS

3.1 | Xylem pressures of intact plants in the field

The water potential of transpiring leaves at midday was −1.27 MPa (ranging from −1.69 to −0.78, n = 18). The water potential of nontranspiring (covered) leaves at midday was −0.91 MPa (ranging from −1.59 to −0.36, n = 18). The mean pressure drop between stem and leaves was 0.36 MPa.

3.2 | Direct comparison shows differences among methods

The direct comparison of VC construction techniques revealed some differences among them (Figure 1). There was no difference between curves constructed by the Dehy-CondApp and Cent-CondApp

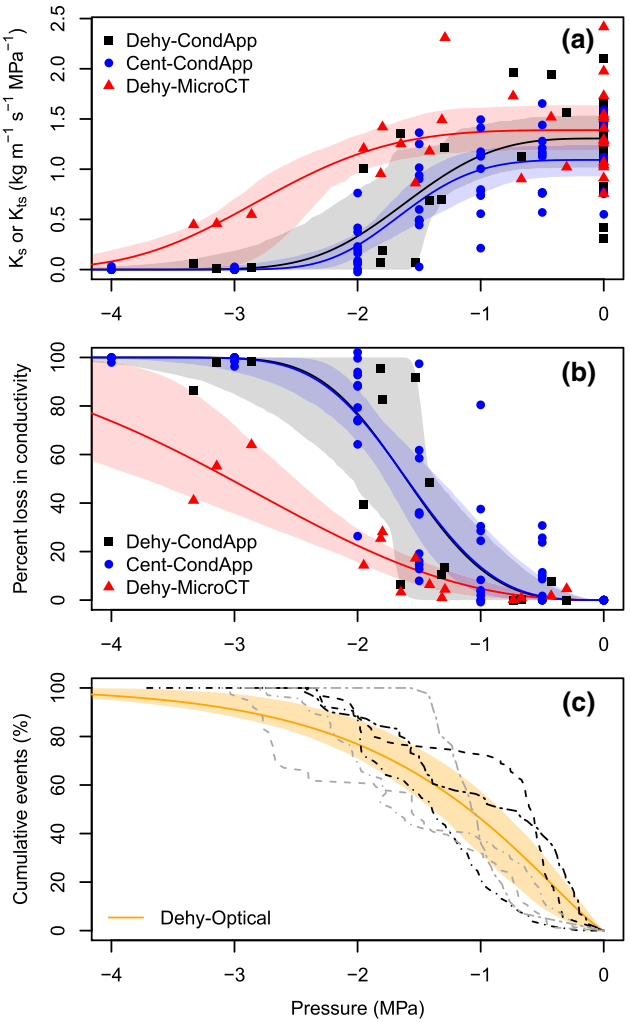

FIGURE 1 Vulnerability curves constructed for black cottonwood (*Populus trichocarpa*) with four different techniques. (a) Hydraulic specific conductivity (K_s) drops in relation to xylem pressure for dehydration plus conductivity apparatus (Dehy-CondApp; black square), dehydration plus high-resolution computer tomography (Dehy-MicroCT; red triangle), and centrifuge plus conductivity apparatus (Cent-CondApp; blue circle) techniques. Theoretical K_s calculations (K_{ts}) based on Hagen–Poiseuille equation are plotted for Dehy-MicroCT. (b) Same vulnerability curves as represented in panel (a) but shown as percent loss in hydraulic conductivity. (c) Vulnerability curve showing the cumulative percent of optical events observed as xylem pressure drops due to air dehydration measured with the optical technique (Dehy-Optical). Individual optical curves are represented (black and grey dashed lines). Best fit curves and 95% confidence intervals obtained by bootstrapping are represented in all panels as solid lines and shaded areas (Dehy-CondApp, black; Dehy-MicroCT, red; Cent-CondApp, blue; Dehy-Optical, orange). Dehy-CondApp and Dehy-MicroCT curves were constructed with the same samples (n = 15), and similar samples in age and size were used for Cent-CondApp (n = 12) and Dehy-Optical (n = 6) techniques

methods. Their best fit curves had nearly identical parameters (Table 2), and their 95% CIs overlapped over the whole of the pressure range (Figure 1a,b). These two curves induced cavitation with different methods (air dehydration vs. centrifugation) and evaluated losses in conductivity with hydraulic measures using the conductivity apparatus. The Dehy-MicroCT VC was significantly different from both the Dehy-CondApp and Cent-CondApp curves, diverging from them at xylem pressures more negative than −1.8 MPa (Figure 1a,b). The Dehy-MicroCT curve implied greater resistance to cavitation than the Dehy-CondApp and Cent-CondApp curves. The maximum PLC estimated by Dehy-MicroCT was 64.0%, whereas the same sample showed 98.4 PLC with the Dehy-CondApp method. Consistent with this pattern, the P_{50} of Dehy-MicroCT was significantly more negative (Table 2).

Significant relationships were observed between hydraulic conductivity measurements performed with the conductivity apparatus and microCT on the same stem segments (Figure 2). The microCT K_{ts} and conductivity apparatus K_s relationship was fitted with a logarithmic function (.002; Figure 2a). MicroCT K_{ts} measurements were generally higher than conductivity apparatus K_s ones. This was more noticeable for low K_s values (Figure 2a), which correspond to more dehydrated samples (Figure 1a). The relationship between K_{smax} and K_{tsmax} was only marginally significant (.097; Figure 2b). Half of microCT K_{tsmax} values were higher than conductivity apparatus K_s ones, and the mean microCT K_{tsmax}-to-dehydration K_{smax} ratio was 1.3. Theoretical expectations predict that K_{tsmax} should be higher for microCT as no end wall resistance is accounted for in the Hagen–Poiseuille equation. The microCT and conductivity apparatus PLC relationship was explained by an exponential function (p < .0001; Figure 2c). Conductivity apparatus PLC was always higher than microCT PLC.

The optical method does not enable calculating PLC nor K_s. However, if the cumulative percent of events was to be considered equal to PLC, the optical curve suggested greater xylem vulnerability than the other three methods. The six samples measured showed high variability in shape and resistance (dash and dash dot lines, Figure 1c). The best overall fit and 95% CI of the optical curve implied significantly greater vulnerability at pressures above −1.0 MPa (Figure 1c versus Figure 1b), consistent with the optical curve having the lowest Weibull c parameter (Table 2). The events P_{50} was reached at −1.1 MPa, which was the highest P_{50} among the four methods, but did not differ significantly from the dehydration and centrifuge P_{50} (Table 2). The microCT scans performed on the optical method samples when the optical curve was completed showed an interesting pattern, with the fibers close to the cambium of debarked areas filled with gas (Figure 3). This contrasted with the outer band of fibers from the area where the bark had not been removed, which remained fluid filled despite samples being highly dehydrated, both in the cross section where the stem was debarked and in the cross-sections distal from the debarked area (Figure 3a,b). The outer band of fibers also remained fluid filled in highly dehydrated samples from the Dehy-MicroCT curve, even after being gas dried for measuring K_{tsmax} (Figure 3c).

3.3 | Single-spin test of hydraulic and microCT methods

The discrepancy between the Cent-CondApp and Dehy-MicroCT VCs at low water potentials (Figure 1) was confirmed with a centrifuge single-spin test at −3.0 MPa (Figure 4a,b). The conductivity apparatus

TABLE 2 Best fit vulnerability curve parameters

Technique	Weibull b	Weibull c	P_{50} [95% CI]* (MPa)	K_{smax} or K_{tsmax} [95% CI]* (kg m^{-1} s^{-1} MPa^{-1})
For specific conductivity (K_s or K_{ts}) curves				
Dehy-CondApp	1.82	3.28	−1.63 [−2.20, −1.34]^a	1.39 [1.01, 1.53]^a
Cent-CondApp	1.80	4.02	−1.65 [−1.82, −1.38]^a	1.09 [0.93, 1.25]^a
Dehy-MicroCT	3.06	3.90	−2.79 [−3.08, −2.29]^b	1.39 [1.19, 1.64]^a
For percent loss in conductivity or percent of events curves				
Dehy-CondApp	1.79	3.41	−1.61 [−2.05, −1.36]^a	
Cent-CondApp	1.79	3.29	−1.60 [−1.79, −1.34]^a	
Dehy-MicroCT	3.54	2.39	−3.04 [−3.74, −2.51]^b	
Dehy-Optical	1.47	1.24	−1.10 [−1.39, −0.84]^a	

Abbreviation: CI, confidence interval.

*Significant differences among techniques (no overlap between 95% confidence intervals) for P_{50} and K_{smax} are shown with different superscript letters.

measurement of K_s was significantly lower than the microCT K_{ts} estimate (paired *t* test, two-tailed 0.046; Figure 4a). Consistent with this result, PLC obtained from the conductivity apparatus was higher than the microCT estimate (paired *t* test, two-tailed 0.016; Figure 4b). Paired *t* tests indicated that there was no difference in K_s (two-tailed 0.275) nor PLC (two-tailed 0.676) between conductivity apparatus measurements performed on the whole 14-cm and central 4.5-cm segments (Figure 4a vs. 4c and 4b vs. 4d). There were no differences among single spin (n = 6) and full centrifuge curve (n = 10) K_s (MWRST, 0.42) and PLC (MWRST, 0.42) measurements at −3.0 MPa (centrifuge, Figure 1a,b, vs. conductivity apparatus, Figure 4a,b). The range of microCT PLC for the single spin (mean PLC 95% CI = 61.7 [37.8, 88.7]) was comparable with the values obtained from bootstrapping for the microCT dehydration curve at −3.0 MPa (PLC = 48.9 [35.5, 72.2]). This indicates that losses in conductivity induced by dehydration and centrifugation for this single-spin curve were consistent with our prior VCs. Importantly, both these stems were fully cut prior to sampling, so the differences between the methods cannot be explained by a cutting effect.

The loss in conductivity profile measured with the conductivity apparatus within the 14-cm–centrifuged stem, evaluated by dividing each stems into three 4.5-cm segments, was consistent with theoretical expectations based on the pressure profile during centrifugation (Figure 4c,d). The central segment showed lower K_s than the proximal and distal ends (ANOVA, 0.001; Figure 4c), and there was no difference between the proximal and distal ends (Tukey's Honest Significant Difference test, 0.38). There was no difference in K_{smax} (measured after flushing) among the three stem positions (ANOVA, 0.21). The PLC of the central segment was significantly higher than PLC from the proximal and distal ends (Kruskal–Wallis one-way analysis of variance on ranks, 0.003; Figure 4d).

3.4 | MicroCT scanning did not impact hydraulic conductivity measures

There was no change in native K_h before and after scanning, 0.94 ± 44 versus 1.27 ± 45 mg m s^{-1} MPa^{-1} (n = 3, paired *t* test, 0.29), indicating that scanning prior to measuring native K_h as described above was not likely to have altered stem conductivity measures.

3.5 | Vessels of the primary xylem were more vulnerable than those of secondary xylem

Primary xylem vessels were significantly more vulnerable than secondary xylem as revealed by microCT image analysis (Figure 5). The mean contribution of primary xylem vessels to total K_{tsmax} was 12.6% (*SE* = 1.6). Therefore, primary xylem has a minor impact on the whole stem VC (as shown by the comparison of Dehy-MicroCT curve in Figure 1b vs. secondary xylem curve in Figure 5a).

4 | DISCUSSION

We found significant differences among VCs constructed with four different techniques, with similar results for Dehy-CondApp and Cent-CondApp VCs, increased resistance in the Dehy-MicroCT curve, and a trend for the Dehy-Optical curve to be more vulnerable than the other methods. These differences are generally consistent with theoretical predictions based on method differences. This is an interesting result given that a very short-vesselled model tree species was sampled, and several studies report no differences among VCs constructed with different techniques for angiosperm species with relatively short vessels (e.g., Choat et al., 2016; Jacobsen, Pratt, Davis, & Tobin, 2014; Li, Sperry, Bush, & Hacke, 2008; Losso et al., 2019). A comparison of each of these methods is discussed further below.

4.1 | Dehydration and centrifuge hydraulic VCs were not different

The Dehy-CondApp and Cent-CondApp curves were not different, which indicates that there was no difference between inducing cavitation by air (benchtop) dehydration or centrifugation. This is similar to many prior studies that have compared dehydration and centrifuge

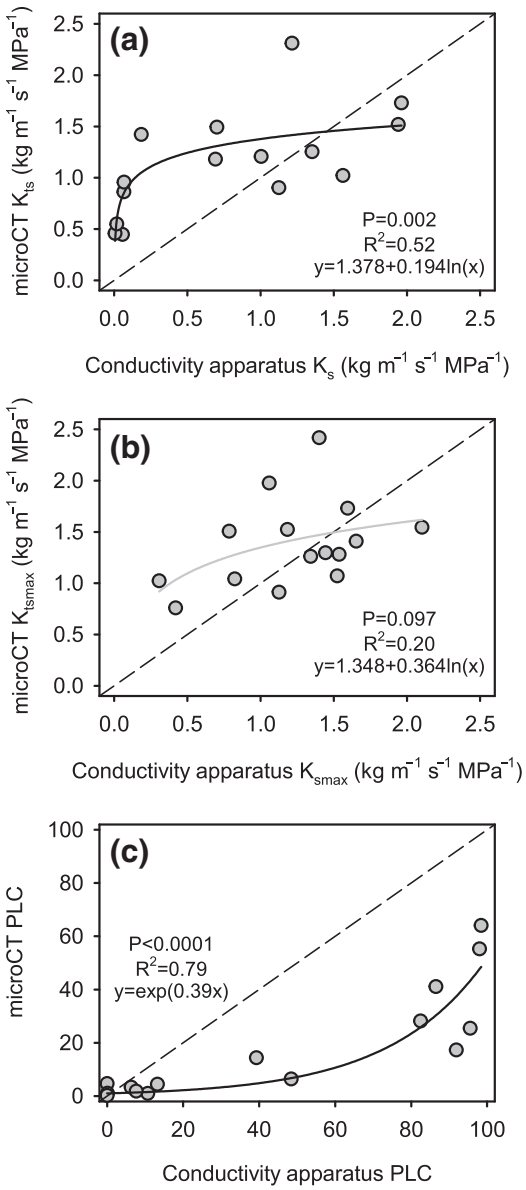

FIGURE 2 Direct comparison of conductivity apparatus and computed microtomography measures performed on the same stems. (a) Native xylem-specific conductivity (K_s) versus native theoretical conductivity (K_{ts}), (b) maximum xylem-specific conductivity (K_{smax}) versus maximum theoretical specific conductivity (K_{tsmax}), and (c) percent loss in conductivity. Regression function, solid line (black for $p < .05$ and grey for $p < .10$); 1:1 relationship, dashed line

curves, especially when the centrifuge curve was based on the use of the standard technique with hydration reservoirs as in the current study (e.g., Hacke et al., 2015; Jacobsen et al., 2014; Sperry et al., 2012; Tobin et al., 2013). Some have found that the centrifuge may produce high embolism in stem ends, particularly if fluid reservoirs are uneven and fluid is flowing through spun samples (as in the Cavitron flow centrifuge technique; Cochard et al., 2005, their figure 5). We tested for this pattern and found that PLC was highest in the centre of segments and not at stem ends, suggesting that this was not an issue in the present study and consistent with other tests using similar methods (Sperry et al., 2012; Tobin et al., 2013).

4.2 | MicroCT VCs appear overly resistant compared with hydraulic VCs

The Dehy-MicroCT curve implied greater resistance to cavitation than the one obtained with the conductivity apparatus (Dehy-CondApp) for the exact same samples. This trend has been observed previously in several studies mainly in long-vesselled species (e.g., Choat et al., 2016; Gleason et al., 2017; López et al., 2018); thus, differences between microCT and centrifuge VCs have often been attributed to a proposed "open-vessel artefact" (e.g., Cochard et al., 2013; López et al., 2018). We performed vessel length measurements on branches equivalent in size and location from the same trees as the ones used for the VCs. On the basis of the silicone injection technique, the median vessel length estimate was 2.57 cm, and for a microCT 3-dimensional (3D) vessel length analysis, which produces a value more indicative of the length distribution within the xylem tissue, the median vessel length was only 0.56 cm (Jacobsen et al., 2019). Of six injected stem segments, only two segments contained any vessels that were longer than 14 cm (only one vessel in each of these two stems from among an average of 2,062 vessels at the point of silicone injection). Thus, the stem segments we used for the centrifuge curves were 14-cm long, over 5× longer than the median vessel length, and most samples contained no open vessels through the measured segment. Thus, our results are not explained by an open-vessel artefact. Moreover, the Dehy-CondApp curve was not different from the Cent-CondApp curve; thus, results were not dependent on the method in which cavitation was induced as would be predicted if there was a centrifuge-associated open–vessel artefact.

Differences between the microCT and conductivity methods cannot be attributed to sample excision (Wheeler, Huggett, Tofte, Fulton, & Holbrook, 2013) because the samples were prepared by excising them under water, trimming back the cut ends following the relaxation of xylem tensions, and finally shaving sample ends with a razor, which has been shown not to induce cavitation (Venturas et al., 2015). Moreover, if the difference observed between Dehy-MicroCT and Dehy-CondApp curves was induced by excision, we would not have observed the same difference between hydraulic measurements and microCT in the single-spin experiment where samples were already fully excised when scanned in the microCT.

Another potential source of discrepancy between microCT and hydraulic measurements is if not all conduits observed in a cross section contribute to K_{tmax} because they are not fully mature or they are permanently occluded by gel or gums (Jacobsen & Pratt, 2012; Pratt & Jacobsen, 2018). This was not the case in this study as active xylem staining and fluorescence imaging indicated that the whole xylem cross section was potentially functional at the time the study was performed. Additionally, a subset of stem segments that were fed an iodine tracer into their xylem to mark conductive vessels showed that vessels were conductive throughout the xylem, including very near the vascular cambium (reported in Jacobsen et al., 2019).

These results indicate that differences among VCs reside not in the technique used for inducing cavitation, that is, dehydration or centrifugation, but in the method used for evaluating embolism, that is,

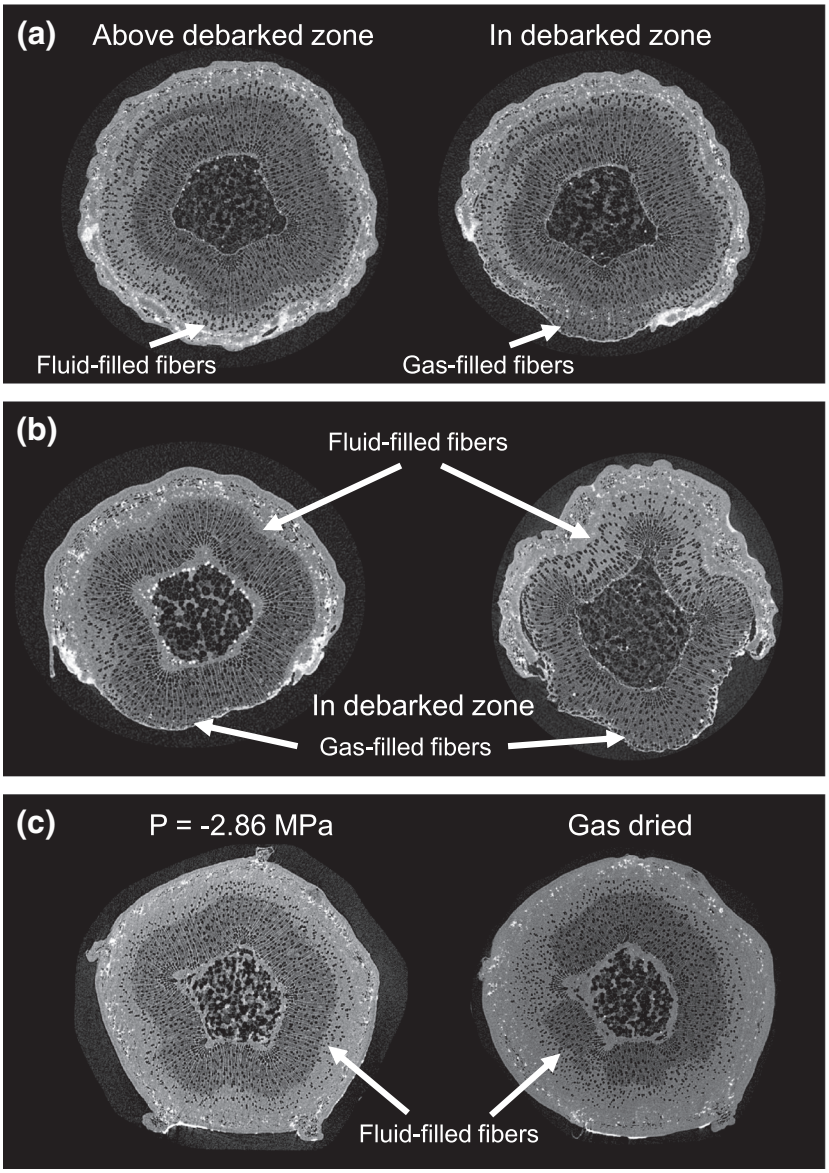

FIGURE 3 Representative computed microtomography images of stems following their use in Dehy-Optical and Dehy-MicroCT method measurements. Stems must be debarked for the optical method, which may change the response of the tissue when it dehydrates. This figure shows three of our six sampled optical stems to illustrate a pattern, namely, that the fibers fill with gas in the debarked region. We observed this in a sample where we scanned just above the debarked region and found that fibers near the cambium appeared as white/light grey indicating that they were fluid filled or living (a, left image) and this differed from the appearance of fibers near the cambium in the debarked zone of the same stem, in which the fibers have dark lumens indicative of being gas filled (a, right image). This same pattern was generally observed across all Dehy-Optical method samples and is apparent in scans of the debarked region from two additional representative samples (b). All of these stems were maximally dehydrated, and the presence of fluid in the fibers may indicate that they are living. Another indication of this is that they were always located nearest to the vascular cambium making them the youngest fibers that may still be developing. Samples used for the Dehy-MicroCT versus Dehy-CondApp curve comparison (which were not debarked) had an outer ring of fluid-filled fibers even when they were highly dehydrated (c, left image) and after being gas dried (c, right image)

conductivity apparatus versus microCT image analysis. The conductivity apparatus directly measures pressure-driven flow through a segment. Thus, these measurements integrate the impact of the 3D structure of the vessel network and the effect of emboli being located in different parts of the conductive pathway. On the other hand, the microCT curve, as analysed here and in other studies, is based on a 2-dimensional (2D) cross-section analysis with conductivity estimated through theoretical calculations. This 2D analysis does not account for resistance from pit membranes, end walls, perforation plates, conduit tapering, and conduit sculpturing, which can represent a significant hydraulic resistance (Schulte, Gibson, & Nobel, 1987; Sperry & Hacke, 2004; Sperry, Hacke, & Wheeler, 2005; Tyree & Ewers, 1991), and does not consider the differential effects of emboli being located in different parts of the network.

MicroCT is a powerful technique that allows visualizing which conduits are gas filled, and this can be quite informative (such as in our comparison of primary and secondary xylem resistance in the present study), but translating this information into hydraulic conductance is challenging. Modelling studies suggest that total hydraulic failure can be reached when there is still a substantial proportion of vessels containing water; however, these are isolated and cannot contribute to water transport (Jacobsen & Pratt, 2018; Loepfe, Martinez-Vilalta, Pinol, & Mencuccini, 2007; Mrad et al., 2018), which is consistent with our results. Greater vascular sectoriality (Orians, van Vuuren, Harris, Babst, & Ellmore, 2004; Zanne, Sweeney, Sharma, & Orians, 2006) and less integrated vessel networks could potentially enhance these differences. Despite the 3D network connectivity not being taken into account when microCT theoretical calculations are performed, this could be incorporated into models if more detailed anatomical information is known (e.g., pit membrane resistance, connectivity, and spatial distribution of emboli; Mrad et al., 2018) and microCT is used to construct 3D models of the conduits network (e.g., Brodersen et al.,

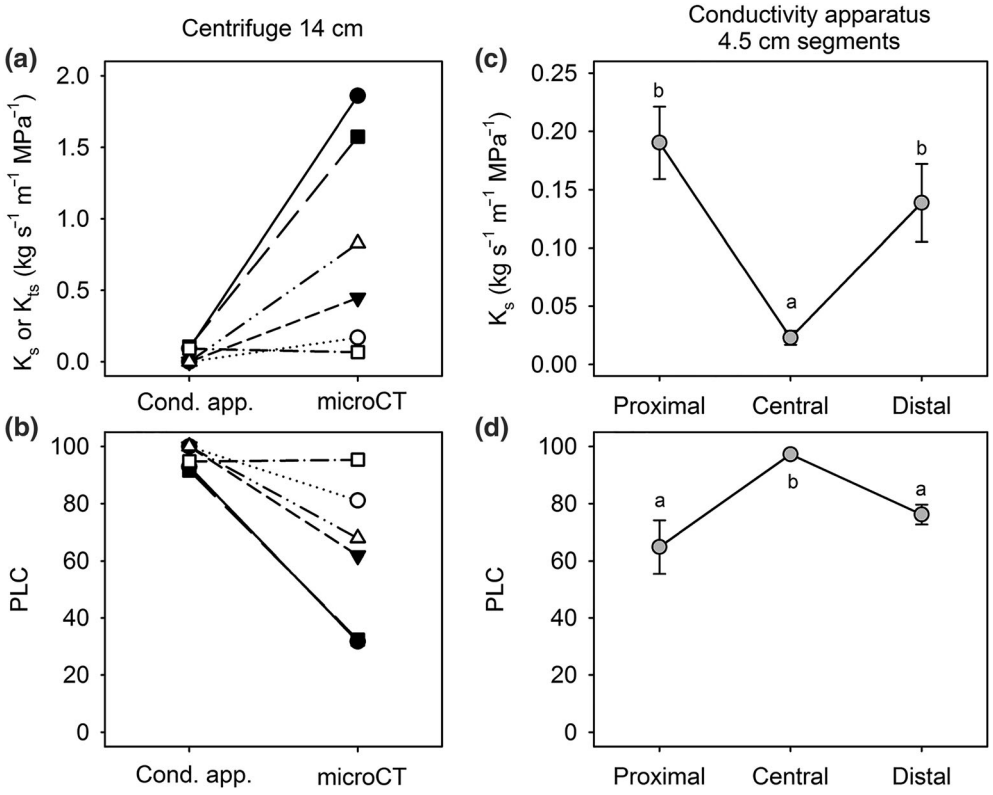

FIGURE 4 Centrifuge single-spin test. (a) Direct comparison of specific conductivity at −3-MPa xylem pressure measured with the conductivity apparatus (K_s) and calculated from computed microtomography (K_{ts}) for 14-cm segments. (b) Conductivity apparatus versus computed microtomography percent loss in conductivity of the 14-cm segments. (c) Conductivity apparatus K_s and (d) percent loss in conductivity of the proximal, central, and distal 4.5-cm segments excised from the 14-cm segments spun in the centrifuge. Error bars in (c) and (d) show ±1 *SE* (n = 6); different letters indicate significant differences among groups (Tukey's Honest Significant Difference test, p < .05)

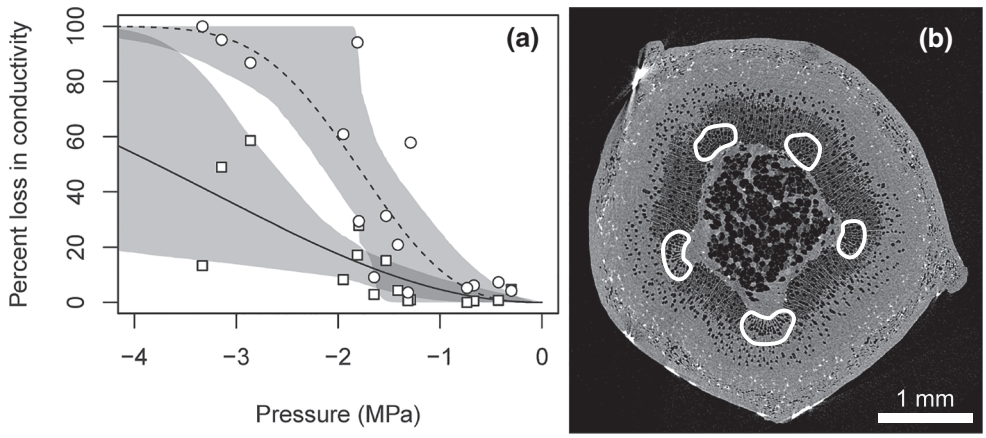

FIGURE 5 Comparison of vulnerability to cavitation of primary (circles) versus secondary xylem vessels (squares). (a) The percent loss in conductivity was calculated from theoretical conductivity from the computed microtomography images. Lines represent the best Weibull fit to the data (primary vessels, dashed; secondary vessels, solid), and shaded areas represent the 95% confidence intervals for these fits. (b) Example of a computed microtomography image processed for automatic analysis from a gas-dried sample showing the regions where primary xylem vessels are located (highlighted with a white contour)

2011; Schulte et al., 1987; Stuppy, Maisano, Colbert, Rudall, & Rowe, 2003). In addition, curves can be calibrated with hydraulic measurements; that is, for a given network and species, there is a relationship that should arise between K_s and PLC measured hydraulically and K_{ts} and PLC estimated through microCT; however, such relationships were not straightforward for the *P. trichocarpa* stems sampled here (Figure 2).

4.3 | Optical VCs provide less information than other techniques and are not easily comparable

The optical method produced highly variable curves, which in general pointed to greater vulnerability to cavitation than the other VC methods. Some of the individual optical curves tended to be r-shaped, and the function providing the best fit to all six samples was r-shaped, which is a shape mistrusted by some researchers (e.g., Cochard & Delzon, 2013; Cochard et al., 2013; Skelton et al., 2018). The optical method records the cavitation events that occur on the exposed surface; thus, it is a 2D analysis that provides insights of when these events occur but not their direct effect on water flow. This method is comparable with the acoustic emissions technique in that it records events (Milburn, 1973; Tyree, Dixon, Tyree, & Johnson, 1984), but it is different in that the optical method only captures events produced close to the xylem surface where light can penetrate, whereas the acoustic technique can measure a larger tissue volume.

An additional disadvantage of the optical technique is that it can record events that are not due to conduit cavitations, similarly to the acoustic emissions technique (Kikuta, Lo Gullo, Nardini, Richter, & Salleo, 1997). Changes in optical reflectance may be caused by fibers or parenchyma dehydrating and not only by vessels cavitating. This would be particularly problematic in species such as the cottonwood we measured, where the size of small vessels overlaps with the size of large fibers (Jacobsen et al., 2019). This may be one of the reasons that optical VCs yielded greater apparent vulnerability to cavitation at high water potentials than the other methods. Future research analysing when fibers empty during the construction of optical VCs could shed light on this potential impact on measurements. Fiber dehydration may occur at different overall dehydration levels for different species.

Compared with microCT, the optical method has the additional disadvantage that it does not allow the calculation of theoretical conductivity. We gave each optical event equal weight for constructing the optical VC, irrespective of the amount of pixels within each event. With automated image analysis, larger pixel areas can represent larger losses of conductivity (Brodribb et al., 2017), but this method is similarly limited because it assumes equal conductivity losses for each pixel. These analyses do not account for flow through a conduit being proportional to its diameter to the fourth power based on Hagen–Poiseuille equation nor are other hydraulic resistances incorporated. The optical curves were scaled to the maximum number of events reached when leaves wilted and no more events were observed in the video (100% of optical events). This is based on the assumption that 100% of optical events correspond to 100 PLC (Brodribb et al., 2017), which can also lead to discrepancy between curves if it is not the case even if losses in conductivity were proportional to the number of optical events. Differences can also arise if samples already have substantial levels of native embolism, which would lead to no optical events until a previously minimum xylem pressure is reached, similar to when flushed versus nonflushed hydraulic PLC curves are compared (Sperry et al., 2012; Venturas et al., 2017). However, this is not likely to have had a large effect in our study because samples presented limited native embolism based on Dehy-MicroCT and Dehy-CondApp curves for pressures above the minimum in situ xylem pressures measured (−0.91 MPa; Figure 1b,c).

One of the chief advantages suggested of the optical method is that it is non-invasive (Skelton et al., 2018); however, our data suggest otherwise. The assumption that debarking to expose xylem for image capture does not affect xylem function (Brodribb et al., 2017; Rodriguez-Dominguez, Carins Murphy, Lucani, & Brodribb, 2018) may require further testing. We found that fibers adjacent to cambium in the debarked area were filled with gas at the conclusion of our optical curves. This pattern differed from the status of fibers within nondebarked zones and suggests that a further limitation of the optical technique may be damage to xylem caused by debarking that alters that xylem tissue response to dehydration.

5 | CONCLUSIONS

Understanding differences among VC methods is critical for interpreting experimental results and advancing knowledge in the fields of plant hydraulics and drought ecophysiology. The main sources of differences among these methods are in the information used to evaluate water transport capacity, in the spatial scale of measures (2D versus 3D measures), and in the tissue volume potentially included in measures. Some methods may be complimentary, such as the combination of hydraulic based measures (dehydration and centrifuge VCs), which provide information on tissue conductivity with visual methods that can reveal the 3D pattern of embolism formation (microCT). The optical VC method seems particularly limited for use in measuring stem xylem, as it does not measure conductivity, is not able to be used to reliably measure cell-type patterns of embolism (i.e., fiber versus vessel embolism), and measures only a small region of tissue near the 2D xylem surface. These differences also suggest that VCs obtained with hydraulic measurements are more appropriate for plant parameterization in water flux models (e.g., Mackay et al., 2015; Sperry et al., 2017).

Black cottonwood is a short-vesselled, diffuse-porous species, which is potentially the xylem structure that should provide greater agreement between methods. We did not find that agreement, and ring-porous species, species with other vessel network characteristics, or species with vasicentric tracheids may be prone to even larger differences. Greater variability in the sizes of vessels within the xylem could lead to a great divergence between hydraulic and visual traits, particularly for the optical technique that does not account for variable hydraulic conductance of conduits that differ in size. Although many studies have interpreted difference between VCs to indicate methodological artefacts, it seems that these differences may often be due to differences in the information used to construct VCs. This information may not always produce VCs that agree, but awareness of the causes of these differences could lead to alternative interpretations based on constructively assimilating information provided from different methods. For instance, a large discrepancy between microCT

and hydraulic VCs may indicate a vessel network that is particularly prone to vessel isolation. In contrast, closer agreement between microCT and hydraulic VCs could indicate a more integrated vessel network. Such interpretations provide useful predictions and are consistent with the available data, whereas there appears to be little support for many previously suggested artefacts in explaining VC discrepancies.

ACKNOWLEDGMENTS

National Science Foundation (IOS-1450650 to M.D.V, HRD-1547784 NSF to R.B.P. and A.L.J., IOS-1252232 to A.L.J.); Army Research Office of Department of Defense (68885-EV-REP, W911NF-16-1-0556 to R. B.P.); Natural Sciences and Engineering Research Council of Canada (NSERC Discovery grant to U.G.H.). Authors declare no conflict of interest.

FUNDING

National Science Foundation; Army Research Office of Department of Defense; Natural Sciences and Engineering Research Council of Canada.

ORCID

Martin D. Venturas https://orcid.org/0000-0001-5972-9064
R. Brandon Pratt https://orcid.org/0000-0001-7537-7644
Anna L. Jacobsen https://orcid.org/0000-0001-7830-5590

REFERENCES

Adams, H. D., Zeppel, M. J., Anderegg, W. R., Hartmann, H., Landhäusser, S. M., Tissue, D. T., … McDowell, N. G. (2017). A multi-species synthesis of physiological mechanisms in drought-induced tree mortality. *Nature Ecology & Evolution*, *1*, 1285–1291. https://doi.org/10.1038/s41559-017-0248-x

Alder, N. N., Pockman, W. T., Sperry, J. S., & Nuismer, S. (1997). Use of centrifugal force in the study of xylem cavitation. *Journal of Experimental Botany*, *48*, 665–674. https://doi.org/10.1093/jxb/48.3.665

Alder, N. N., Sperry, J. S., & Pockman, W. T. (1996). Root and stem xylem embolism, stomatal conductance, and leaf turgor in *Acer grandidentatum* populations along a soil moisture gradient. *Oecologia*, *105*, 293–301. https://doi.org/10.1007/BF00328731

Brodersen, C., McElrone, A. J., Choat, B., Matthews, M. A., & Shackel, K. A. (2010). The dynamics of embolism repair in xylem: In vivo visualizations using high-resolution computed tomography. *Plant Physiology*, *154*, 1088–1095. https://doi.org/10.1104/pp.110.162396

Brodersen, C. R., Lee, E. F., Choat, B., Jansen, S., Phillips, R. J., Shackel, K. A., … Matthews, M. A. (2011). Automated analysis of three-dimensional xylem networks using high-resolution computed tomography. *New Phytologist*, *191*, 1168–1179. https://doi.org/10.1111/j.1469-8137.2011.03754.x

Brodribb, T. J., Carriqui, M., Delzon, S., & Lucani, C. (2017). Optical measurement of stem xylem vulnerability. *Plant Physiology*, *174*, 2054–2061. https://doi.org/10.1104/pp.17.00552

Brodribb, T. J., & Cochard, H. (2009). Hydraulic failure defines the recovery and point of death in water-stressed conifers. *Plant Physiology*, *149*, 575–584. https://doi.org/10.1104/pp.108.129783

Choat, B., Badel, E., Burlett, R., Delzon, S., Cochard, H., & Jansen, S. (2016). Noninvasive measurement of vulnerability to drought-induced embolism by X-ray microtomography. *Plant Physiology*, *170*, 273–282. https://doi.org/10.1104/pp.15.00732

Cochard, H., Badel, E., Herbette, S., Delzon, S., Choat, B., & Jansen, S. (2013). Methods for measuring plant vulnerability to cavitation: A critical review. *Journal of Experimental Botany*, *64*, 4779–4791. https://doi.org/10.1093/jxb/ert193

Cochard, H., & Delzon, S. (2013). Hydraulic failure and repair are not routine in trees. *Annales des Sciences Forestieres*, *70*, 659–661. https://doi.org/10.1007/s13595-013-0317-5

Cochard, H., Delzon, S., & Badel, E. (2015). X-ray microtomography (micro-CT): A reference technology for high-resolution quantification of xylem embolism in trees. *Plant, Cell & Environment*, *38*, 201–206. https://doi.org/10.1111/pce.12391

Cochard, H., Gaelle, D., Bodet, C., Tharwat, I., Poirier, M., & Ameglio, T. (2005). Evaluation of a new centrifuge technique for rapid generation of xylem vulnerability curves. *Physiologia Plantarum*, *124*, 410–418. https://doi.org/10.1111/j.1399-3054.2005.00526.x

Dixon, H. H., & Joly, J. (1895). On the ascent of sap. *Philosophical Transactions of the Royal Society of London, Series B: Biological Sciences*, *186*, 563–576.

Fromm, J. H., Sautter, I., Matthies, D., Kremer, J., Schumacher, P., & Ganter, C. (2001). Xylem water content and wood density in spruce and oak trees detected by high-resolution computed tomography. *Plant Physiology*, *127*, 416–425. https://doi.org/10.1104/pp.010194

Gleason, S. M., Wiggans, D. R., Bliss, C. A., Young, J. S., Cooper, M., Willi, K. R., & Comas, L. H. (2017). Embolized stems recover overnight in *Zea mays*: The role of soil water, root pressure, and nighttime transpiration. *Frontiers in Plant Science*, *8*, 662. https://doi.org/10.3389/fpls.2017.00662

Hacke, U. G., Sperry, J. S., & Pittermann, J. (2000). Drought experience and cavitation resistance in six desert shrubs of the Great Basin, Utah. *Basic and Applied Ecology*, *1*, 31–41. https://doi.org/10.1078/1439-1791-00006

Hacke, U. G., Venturas, M. D., MacKinnon, E. D., Jacobsen, A. L., Sperry, J. S., & Pratt, R. B. (2015). The standard centrifuge method accurately measures vulnerability curves of long-vesselled olive stems. *New Phytologist*, *205*, 116–127. https://doi.org/10.1111/nph.13017

Jacobsen, A. L., & Pratt, R. B. (2012). No evidence for an open vessel effect in centrifuge-based vulnerability curves of a long-vesseled liana (*Vitis vinifera*). *New Phytologist*, *194*, 982–990. https://doi.org/10.1111/j.1469-8137.2012.04118.x

Jacobsen, A. L., & Pratt, R. B. (2018). Going with the flow: Structural determinants of vascular tissue transport efficiency and safety. *Plant, Cell & Environment*, *41*, 2715–2717. https://doi.org/10.1111/pce.13446

Jacobsen, A. L., Pratt, R. B., Davis, S. D., & Tobin, M. F. (2014). Geographic and seasonal variation in chaparral vulnerability to cavitation. *Madrono*, *61*, 317–327. https://doi.org/10.3120/0024-9637-61.4.317

Jacobsen, A. L., Pratt, R. B., Venturas, M. D., & Hacke, U. G. (2019). Large volume vessels are vulnerable to water-stress-induced embolism in stems of poplar. *IAWA Journal*, *40*, 4–22. https://doi.org/10.1163/22941932-40190233

Jacobsen, A. L., Valdovinos-Ayala, J., Rodriguez-Zaccaro, F. D., Hill-Crim, M. A., Percolla, M. I., & Venturas, M. D. (2018). Intra-organismal variation in the structure of plant vascular transport tissues in poplar trees. *Trees*, *32*, 1335–1346. https://doi.org/10.1007/s00468-018-1714-z

Kikuta, S. B., Lo Gullo, M. A., Nardini, A., Richter, H., & Salleo, S. (1997). Ultrasound acoustic emissions from dehydrating leaves of deciduous and evergreen trees. *Plant, Cell & Environment*, *20*, 1381–1390. https://doi.org/10.1046/j.1365-3040.1997.d01-34.x

Lewis, A. M., & Boose, E. R. (1995). Estimating volume flow rates through xylem conduits. *American Journal of Botany*, *82*, 1112–1116. https://doi.org/10.1002/j.1537-2197.1995.tb11581.x

Li, Y., Sperry, J. S., Bush, S. E., & Hacke, U. G. (2008). Evaluation of centrifugal methods for measuring xylem cavitation in conifers, diffuse- and ring-porous angiosperms. *New Phytologist*, *177*, 558–568. https://doi.org/10.1111/j.1469-8137.2007.02272.x

Loepfe, L., Martinez-Vilalta, J., Pinol, J., & Mencuccini, M. (2007). The relevance of xylem network structure for plant hydraulic efficiency and safety. *Journal of Theoretical Biology*, *247*, 788–803. https://doi.org/10.1016/j.jtbi.2007.03.036

López, R., Nolf, M., Duursma, R. A., Badel, E., Flavel, R. J., Cochard, H., & Choat, B. (2018). Mitigating the open vessel artefact in centrifuge-based measurement of embolism resistance. *Tree Physiology*, *39*, 143–155. https://doi.org/10.1093/treephys/tpy083

Losso, A., Bär, A., Dämon, B., Dullin, C., Ganthaler, A., Petruzzellis, F., … Mayr, S. (2019). Insights from in vivo micro-CT analysis: Testing the hydraulic vulnerability segmentation in *Acer pseudoplatanus* and *Fagus sylvatica* seedlings. *New Phytologist*, *221*, 1831–1842. https://doi.org/10.1111/nph.15549

Mackay, D. S., Roberts, D. E., Ewers, B. E., Sperry, J. S., McDowell, N., & Pockman, W. (2015). Interdependence of chronic hydraulic dysfunction and canopy processes can improve integrated models of tree response to drought. *Water Resources Research*, *51*, 6156–6176. https://doi.org/10.1002/2015WR017244

McElrone, A. J., Choat, B., Parkinson, D. Y., MacDowell, A. A., & Brodersen, C. R. (2013). Using high resolution computed tomography to visualize the three dimensional structure and function of plant vasculature. *Journal of Visualized Experiments*, *74*, e50162. https://doi.org/10.3791/50162

Mencuccini, M., Manzoni, S., & Christoffersen, B. (2019). Modelling water fluxes in plants: From tissues to biosphere. *New Phytologist*, *222*, 1207–1222. https://doi.org/10.1111/nph.15681

Milburn, J. A. (1973). Cavitation in *Ricinus* by acoustic detection: Induction in excised leaves by various factors. *Planta*, *110*, 253–265. https://doi.org/10.1007/BF00387637

Mrad, A., Domec, J. C., Huang, C. W., Lens, F., & Katul, G. (2018). A network model links wood anatomy to xylem tissue hydraulic behaviour and vulnerability to cavitation. *Plant, Cell & Environment*, *41*, 2718–2730. https://doi.org/10.1111/pce.13415

Nardini, A., Savi, T., Losso, A., Petit, G., Pacilè, S., Tromba, G., … Salleo, S. (2017). X-ray microtomography observations of xylem embolism in stems of *Laurus nobilis* are consistent with hydraulic measurements of percentage loss of conductance. *New Phytologist*, *213*, 1068–1075. https://doi.org/10.1111/nph.14245

Nolf, M., Lopez, R., Peters, J. M., Flavel, R. J., Koloadin, L. S., Young, I. M., & Choat, B. (2017). Visualization of xylem embolism by X-ray microtomography: A direct test against hydraulic measurements. *New Phytologist*, *214*, 890–898. https://doi.org/10.1111/nph.14462

Orians, C. M., van Vuuren, M. M., Harris, N. L., Babst, B. A., & Ellmore, G. S. (2004). Differential sectoriality in long-distance transport in temperate tree species: Evidence from dye flow, 15 N transport, and vessel element pitting. *Trees*, *18*, 501–509. https://doi.org/10.1007/s00468-004-0326-y

Petruzzellis, F., Pagliarani, C., Savi, T., Losso, A., Cavalletto, S., Tromba, G., … Miotto, A. (2018). The pitfalls of in vivo imaging techniques: Evidence for cellular damage caused by synchrotron X-ray computed micro-tomography. *New Phytologist*, *220*, 104–110. https://doi.org/10.1111/nph.15368

Pockman, W. T., Sperry, J. S., & O'Leary, J. W. (1995). Sustained and significant negative water pressure in xylem. *Nature*, *378*, 715–716. https://doi.org/10.1038/378715a0

Pratt, R. B., & Jacobsen, A. L. (2018). Identifying which conduits are moving water in woody plants: A new HRCT-based method. *Tree Physiology*, *38*, 1200–1212. https://doi.org/10.1093/treephys/tpy034

R Core Team (2016). *R: A language and environment for statistical computing*. Vienna, Austria: R Foundation for Statistical Computing.

Rodriguez-Dominguez, C. M., Carins Murphy, M., Lucani, C., & Brodribb, T. J. (2018). Mapping xylem failure in disparate organs of whole plants reveals extreme resistance in olive roots. *New Phytologist*, *218*, 1025–1035. https://doi.org/10.1111/nph.15079

Savi, T., Miotto, A., Petruzzellis, F., Losso, A., Pacilè, S., Tromba, G., … Nardini, A. (2017). Drought-induced embolism in stems of sunflower: A comparison of in vivo micro-CT observations and destructive hydraulic measurements. *Plant Physiology and Biochemistry*, *120*, 24–29. https://doi.org/10.1016/j.plaphy.2017.09.017

Schulte, P. J., Gibson, A. C., & Nobel, P. S. (1987). Xylem anatomy and hydraulic conductance of *Psilotum nudum*. *American Journal of Botany*, *74*, 1438–1445. https://doi.org/10.1002/j.1537-2197.1987.tb08757.x

Skelton, R. P., Dawson, T. E., Thompson, S. E., Shen, Y., Weitz, A. P., & Ackerly, D. (2018). Low vulnerability to xylem embolism in leaves and stems of North American oaks. *Plant Physiology*, *177*, 1066–1077. https://doi.org/10.1104/pp.18.00103

Sparks, J. P., & Black, R. A. (1999). Regulation of water loss in populations of *Populus trichocarpa*: The role of stomatal control in preventing xylem cavitation. *Tree Physiology*, *19*, 453–459. https://doi.org/10.1093/treephys/19.7.453

Sperry, J. S. (1986). Relationship of xylem embolism to xylem pressure potential, stomatal closure, and shoot morphology in the palm *Rhapis excelsa*. *Plant Physiology*, *80*, 110–116. https://doi.org/10.1104/pp.80.1.110

Sperry, J. S., Christman, M. A., & Smith, D. D. (2012). Vulnerability curves by centrifugation: Is there an open vessel artifact, and are "r" shaped curves necessarily invalid? *Plant, Cell & Environment*, *35*, 601–610. https://doi.org/10.1111/j.1365-3040.2011.02439.x

Sperry, J. S., Donnelly, J. R., & Tyree, M. T. (1988). A method for measuring hydraulic conductivity and embolism in xylem. *Plant, Cell & Environment*, *11*, 35–40. https://doi.org/10.1111/j.1365-3040.1988.tb01774.x

Sperry, J. S., & Hacke, U. G. (2004). Analysis of circular bordered pit function I. Angiosperm vessels with homogenous pit membranes. *American Journal of Botany*, *91*, 369–385. https://doi.org/10.3732/ajb.91.3.369

Sperry, J. S., Hacke, U. G., Oren, R., & Comstock, J. P. (2002). Water deficits and hydraulic limits to leaf water supply. *Plant, Cell & Environment*, *25*, 251–263. https://doi.org/10.1046/j.0016-8025.2001.00799.x

Sperry, J. S., Hacke, U. G., & Wheeler, J. K. (2005). Comparative analysis of end-wall resistance in xylem conduits. *Plant, Cell & Environment*, *28*, 456–465. https://doi.org/10.1111/j.1365-3040.2005.01287.x

Sperry, J. S., & Love, D. M. (2015). What plant hydraulics can tell us about plant responses to climate-change droughts. *New Phytologist*, *207*, 14–27. https://doi.org/10.1111/nph.13354

Sperry, J. S., & Tyree, M. T. (1988). Mechanism of water stress-induced xylem embolism. *Plant Physiology*, *88*, 581–587. https://doi.org/10.1104/pp.88.3.581

Sperry, J. S., Venturas, M. D., Anderegg, W. R., Mencuccini, M., Mackay, D. S., Wang, Y., & Love, D. M. (2017). Predicting stomatal responses to the environment from the optimization of photosynthetic gain and hydraulic cost. *Plant, Cell & Environment*, *40*, 816–830. https://doi.org/10.1111/pce.12852

Stuppy, W. H., Maisano, J. A., Colbert, M. W., Rudall, P. J., & Rowe, T. B. (2003). Three-dimensional analysis of plant structure using high-

resolution X-ray computed tomography. *Trends in Plant Science*, *8*, 2–6. https://doi.org/10.1016/S1360-1385(02)00004-3

Tobin, M. F., Pratt, R. B., Jacobsen, A. L., & De Guzman, M. E. (2013). Xylem vulnerability to cavitation can be accurately characterised in species with long vessels using a centrifuge method. *Plant Biology*, *15*, 496–504. https://doi.org/10.1111/j.1438-8677.2012.00678.x

Tyree, M. T., Alexander, J., & Machado, J. L. (1992). Loss of hydraulic conductivity due to water stress in intact juveniles of *Quercus rubra* and *Populus deltoides*. *Tree Physiology*, *10*, 411–415. https://doi.org/10.1093/treephys/10.4.411

Tyree, M. T., Dixon, M. A., Tyree, E. L., & Johnson, R. (1984). Ultrasonic acoustic emissions from the sapwood of cedar and hemlock: An examination of three hypotheses regarding cavitations. *Plant Physiology*, *75*, 988–992. https://doi.org/10.1104/pp.75.4.988

Tyree, M. T., & Ewers, F. W. (1991). The hydraulic architecture of trees and other woody plants. *New Phytologist*, *119*, 345–360. https://doi.org/10.1111/j.1469-8137.1991.tb00035.x

Tyree, M. T., & Sperry, J. S. (1988). Do woody plants operate near the point of catastrophic xylem dysfunction caused by dynamic water stress? Answers from a model. *Plant Physiology*, *88*, 574–580. https://doi.org/10.1104/pp.88.3.574

Venturas, M. D., MacKinnon, E. D., Jacobsen, A. L., & Pratt, R. B. (2015). Excising stem samples underwater at native tension does not induce xylem cavitation. *Plant, Cell & Environment*, *38*, 1060–1068. https://doi.org/10.1111/pce.12461

Venturas, M. D., Rodriguez-Zaccaro, F. D., Percolla, M. I., Crous, C. J., Jacobsen, A. L., & Pratt, R. B. (2016). Single vessel air injection estimates of xylem resistance to cavitation are affected by vessel network characteristics and sample length. *Tree Physiology*, *36*, 1247–1259. https://doi.org/10.1093/treephys/tpw055

Venturas, M. D., Sperry, J. S., & Hacke, U. G. (2017). Plant xylem hydraulics: What we understand, current research, and future challenges. *Journal of Integrative Plant Biology*, *59*, 356–389. https://doi.org/10.1111/jipb.12534

Venturas, M. D., Sperry, J. S., Love, D. M., Frehner, E. H., Allred, M. G., Wang, Y., & Anderegg, W. R. (2018). A stomatal control model based on optimization of carbon gain versus hydraulic risk predicts aspen sapling responses to drought. *New Phytologist*, *220*, 836–850. https://doi.org/10.1111/nph.15333

Wang, R., Zhang, L., Zhang, S., Cai, J., & Tyree, M. T. (2014). Water relations of *Robinia pseudoacacia* L.: Do vessels cavitate and refill diurnally or are R-shaped curves invalid in Robinia? *Plant, Cell & Environment*, *37*, 2667–2678. https://doi.org/10.1111/pce.12315

Wheeler, J. K., Huggett, B., Tofte, A., Fulton, R., & Holbrook, N. M. (2013). Cutting xylem under tension or supersaturated with gas can generate PLC and the appearance of rapid recovery from embolism. *Plant, Cell & Environment*, *36*, 1938–1949. https://doi.org/10.1111/pce.12139

Zanne, A. E., Sweeney, K., Sharma, M., & Orians, C. M. (2006). Patterns and consequences of differential vascular sectoriality in 18 temperate tree and shrub species. *Functional Ecology*, *20*, 200–206. https://doi.org/10.1111/j.1365-2435.2006.01101.x

Zimmermann, M. H. (1983). *Xylem structure and the ascent of sap*Springer, Berlin Heidelberg New York.

SUPPORTING INFORMATION

Additional supporting information may be found online in the Supporting Information section at the end of the article.

Figure S1. Comparison counts of cavitation event from the same optical stem evaluated by three different researchers.

How to cite this article: Venturas MD, Pratt RB, Jacobsen AL, Castro V, Fickle JC, Hacke UG. Direct comparison of four methods to construct xylem vulnerability curves: Differences among techniques are linked to vessel network characteristics. *Plant Cell Environ*. 2019;42:2422–2436. https://doi.org/10.1111/pce.13565